

Plasmonic Electro-Optic Modulators - A Review

Review Article**Author(s):**

Smajic, Jasmin ; Leuthold, Juerg 

Publication date:

2024

Permanent link:

<https://doi.org/10.3929/ethz-b-000676569>

Rights / license:

[Creative Commons Attribution 4.0 International](#)



Originally published in:

IEEE Journal of Selected Topics in Quantum Electronics 30(4), <https://doi.org/10.1109/JSTQE.2024.3396549>

Funding acknowledgement:

899558 - attojoule Cryogenic Communication (EC)

Plasmonic Electro-Optic Modulators – A Review

J. Smajic , Senior Member, IEEE, and J. Leuthold 

Abstract—Electro-optical modulators are key components in photonic communications, and they are decisively important for the quality and data transmission rates. They encode information by modulating the amplitude, phase, frequency or polarization of an optical wave in response to an electrical field. This paper offers a detailed review on plasmonic modulators, their structure, variations, capabilities, and figures of merit.

Index Terms—Plasmonics, modulators, integrated optics.

I. INTRODUCTION

ELECTRO-OPTICAL (EO) modulators bridge the electrical and optical world in optical communications systems [1]. Data are usually generated and received in the electronic world, but transmission is performed in the optical domain. Meanwhile electro-optical modulators encode data for transoceanic links but as well for short reach interconnects in data centers. Soon, they are expected to encode data for on-chip optical interconnects [2], [3]. Beyond communications, electro-optical modulators are increasingly pivotal in sensing high frequency radio [4] or THz signals [5].

Ultimately, the success of electro-optical modulators depends on a few performance factors. Among which are a high frequency response, low power consumption, low optical losses, thermal stability, a small footprint, the extinction ratio, integrateability with CMOS but also ease of fabrication and cost [1], [6].

The operating principle of an EO modulator relays either on an electro-refraction (ER) effect, or on an electro-absorption (EA) effect. While the former effect exploits an external electric field for changing the refractive index of the optical medium (the Pockels effect [1] - also known as the linear-electro optical effect, the quadratic Kerr effect, or the plasma dispersion effect), the later effect utilizes an external field for changing absorption in semiconductors (the Franz-Keldish effect, quantum confined Stark effect, or free-carrier absorption) [6], [7].

Manuscript received 2 February 2024; revised 16 April 2024; accepted 27 April 2024. Date of publication 3 May 2024; date of current version 28 May 2024. This work was supported in part by EU Project: Agile uLtra Low EnerGy secuRe netwOrks (ALLEGRO), under Grant 101092766, in part by EU Project: Flexibly Scalable Energy Efficient Networking (FLEX-SCALE), under Grant 101096909, in part by InnoSuisse Project: Ultra-Miniature Wideband 5G & 6G Electromagnetic Radiation Sensor (5&6-GEARS), under Grant 53099.1 IP-ICT, and in part by EU Project: attojoule Cryogenic Communication (aCryComm), under Grant 899558. (Corresponding authors: J. Smajic; J. Leuthold.)

The authors are with the Institute of Electromagnetic Fields, ETH, 8092 Zurich, Switzerland (e-mail: smajicj@ethz.ch; leuthold@ethz.ch).

Color versions of one or more figures in this article are available at <https://doi.org/10.1109/JSTQE.2024.3396549>.

Digital Object Identifier 10.1109/JSTQE.2024.3396549

Silicon photonics is presently widely accepted as the most promising platform for developing EO modulators compatible with the standard CMOS fabrication technologies. Due to the absence of the Pockels and Kerr effect in silicon, silicon modulators operate by utilizing the plasma dispersion effect. Despite of its bandwidth limitations [8], this effect in a Mach-Zehnder modulator enables data rates of 70 Gbit/s [9] and reaches even 224 Gbit/s if integrated within more complex configurations and by the help of advanced coding [10]. It is also worth mentioning that there are some intrinsic problems associated with silicon limiting sometimes its applications. For instance, the effect of parasitic two-photon absorption at the wavelength of 1.55 μm (despite of the single photon absorption limit at 1.1 μm in silicon) could be an obstacle in high power applications [11]. Additionally, silicon exhibits a high thermo-optical coefficient, which is a considerable problem for phase-sensitive applications.

To overcome the mentioned speed limitations of the plasma dispersion effect, one may use the Pockels-effect instead. Unfortunately, materials with a sufficiently large Pockels effect are incompatible with silicon. One therefore typically resorts to a hybrid integration of photonics with the nonlinear material. Most prominently, the thin-film lithium-niobate (LiNbO_3) technique has attracted quite some attention. Yet, the nonlinear coefficients of LiNbO_3 are relatively small. BTO offers higher nonlinearity – but at the price of a more complex fabrication [12]. Alternatively, organic materials [1] offer highest electro-optical effects. In response the so-called “silicon-organic hybrid (SOH)” platform has emerged [13], [14]. Here, a silicon slot waveguide is filled with an organic electro-optical (OEO) material offering a high $\chi^{(2)}$ -nonlinear Pockels effect [15]. With this technology data rates of 192 GBd [16] and bandwidths up to 100 GHz [17] have been shown. And while all these hybrid integration approaches have led to remarkable successes, they are all fundamentally low-pass-filter limited. Due to the relatively low level of E-field confinement in the active area, the required length of modulators typically is huge exceeding 100 s and sometimes requiring lengths of 1000 s μm . This results in walk-offs between optical and electrical fields. Such walk-off may be overcome by dispersion engineering of both the RF and optical field. Yet, the RF field will still attenuate if the electrodes are excessively large. Speed is thus fundamentally limited despite of various mitigation techniques [17], [18].

Plasmonic EO modulators capable of subwavelength optical field confinement between the metallic electrodes offer a solution to the bandwidth problems. Plasmonic optical waveguides offer an unprecedented level of E-field confinement in the active modulating region leading to a short modulating path in the order of 10 μm [19], [20]. As a consequence, we can operate

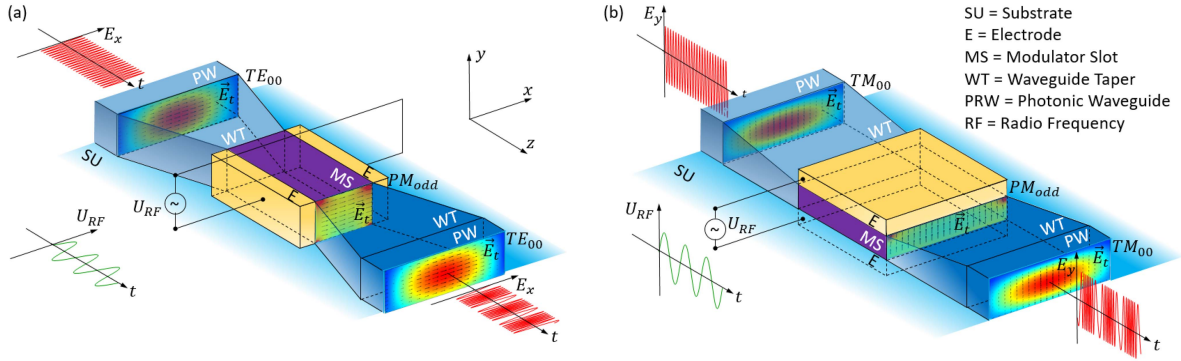


Fig. 1. (a) Horizontal- and (b) vertical-stack arrangement of an EO plasmonic modulator. An optical wave is guided in and out of the modulator by means of silicon photonic waveguides. The active area is confined to a slot within a plasmonic metal-insulator-metal (MIM) waveguide. The size of the photonic mode is adjusted to the plasmonic mode by a tapering section. At the input and output we have depicted an optical continuous wave (CW) input E_x -field component and its phase modulated output counterpart (red). The corresponding RF signal (green) used for phase modulation is also visualized. More details can be found in the text.

them as lumped modulators only speed limited by the RC-time constant and no longer limited by walk-offs [14]. Since these capacities are orders of magnitude lower over the values of traditional modulators, bandwidths in excess of 500 GHz have been consequently measured [4]. Along with this comes an extremely small footprint that can be as small as a few μm^2 for the whole modulator [21]. Also, record low energy consumption in the atto-Joule range have been found [22]. The many advantages of the plasmonic approaches come at the price of higher losses, yet, latest plasmonic ring modulators feature low on-chip losses of 1.2 dB [23] and new low loss approaches emerge [24], [25].

The Pockels-effect may come from a large variety of different electro-optical materials. Historically, electro-optic organic materials were used first, which led to the term “plasmonic organic hybrid (POH)” approach [26]. Meanwhile also ferroelectric BTO and LiNbO_3 plasmonic modulators have emerged [20], [27], [28]. These modulators are of interest when thermal stability might be an issue as they have already shown to sustain temperatures up to 250 °C [20]. More recently, plasmonic modulators have been fabricated on the silicon nitrate (SiN) platform [27]. The SiN platform promises resilience to high input powers, offers a wider transparency window, thermal robustness, lower index contrast between core and cladding and consequently larger fabrication tolerances, and very low propagation losses [29].

This paper focuses on plasmonic EO modulators, presenting in detail their most promising variants, their operating principles, features, figures of merit, and summarizes the most recent results.

The paper is structured and organized by following a top-down approach. Section II presents the physics of the horizontal and vertical stack plasmonic EO modulator. Section III reviews the building blocks of the modulators described in the previous section, i.e., it contains a theoretical basis of a silicon photonic waveguide and its tapering into the modulating slot, a dispersion diagram and modes of a plasmonic horizontal- and vertical slot waveguide, and a theoretical background of surface plasmon polaritons (SPP) essential for the plasmonic modulator. Section IV reviews the modulator features and figures of merit and presents state-of-the-art results. Section V concludes the paper.

II. PLASMONIC WAVEGUIDE STRUCTURES

Plasmonic EO modulators comprise of a metal-insulator-metal waveguide (often called a plasmonic slot-waveguide). They can be realized within a horizontal or vertical stack layout [30], as presented in Fig. 1. The insulator layer then is the active region of the modulator, see Fig. 1(pink). This insulating slot is filled with a Pockels-material, characterized by $\epsilon_r(E)$. In both arrangements, the slot is surrounded by two metallic electrodes. They not only confine the optical field into a plasmonic field but also guide the RF-field used for modulating the optical wave that drops off across the same region.

In the implementation of Fig. 1, the optical wave (carrier) is launched through strip or ridge waveguides into the modulator. Likewise, these waveguides are again used to couple the light back to a fiber.

The field in the modulator can be described by the following equation

$$\vec{E}_t^\omega(\vec{r}_t, L) = \vec{E}_t^\omega(\vec{r}_t, 0) e^{j\beta(\vec{E}^\Omega)L}, \quad (1)$$

where L is the modulator length, $\vec{r}_t = (x, y)^T$ is a position vector of an arbitrary point within a transversal plane at position z ($0 \leq z \leq L$) of the modulator, $\vec{E}_t^\omega(\vec{r}_t, L)$ is the transversal electric field of the optical wave at the end of the modulator’s active region, $\vec{E}_t^\omega(\vec{r}_t, 0)$ is the transversal electric field of the optical wave at the beginning of the active region and $\beta(\vec{E}^\Omega)$ is the propagation constant of the optical wave propagating through the modulator active region. It depends on the electric RF-field \vec{E}^Ω that is due to the RF-voltage U_{RF} dropping off across the electrodes

For guiding light through the modulator, the modulator with its active region and field enhancing electrodes forms a plasmonic optical waveguide. As visible in Fig. 1, the optical strip waveguide is usually considerable larger than the plasmonic waveguide (400 nm vs. 100 nm) which makes waveguide tapering regions necessary before and after the modulator.

To visualize the modulation effect we have depicted a continuous optical wave at the input waveguide (red), a modulating RF-voltage between the electrodes (green), and the corresponding phase-modulated optical wave (red) at the output, see Fig. 1.

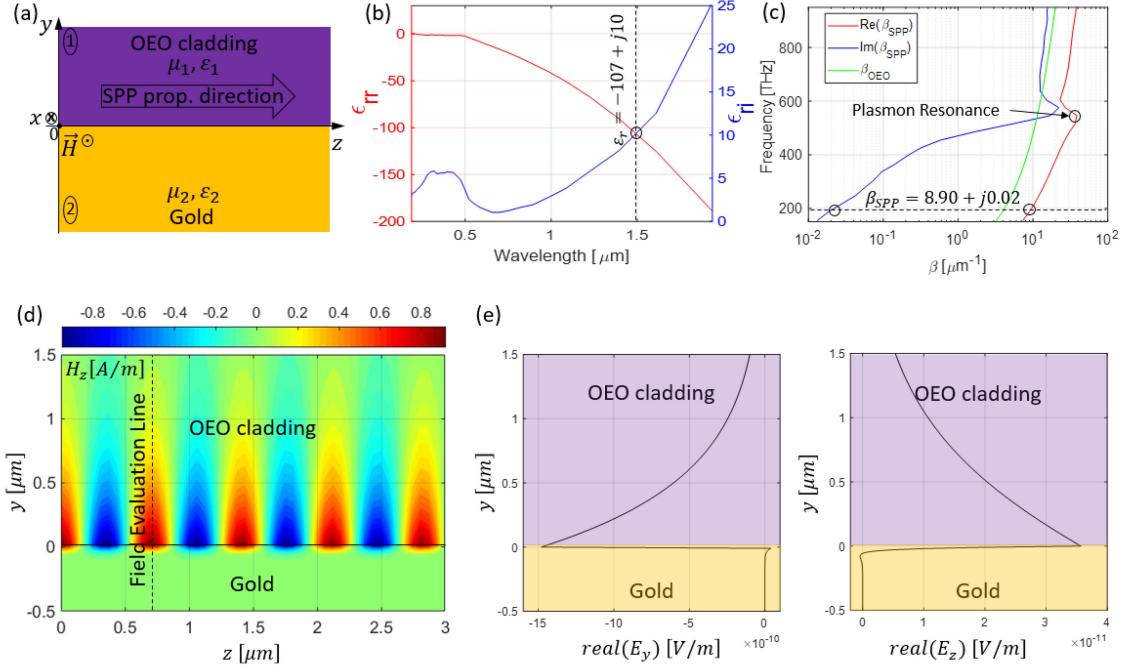


Fig. 2. Excitation of a SPP at the surface of an insulator-metal interface. (a) Figure of the interface with the used materials. (b) Real- and imaginary part of dielectric permittivity of gold versus vacuum wavelength. (c) Dispersion relation of a plasmonic TM-mode at a metal-insulator interface. (d) The magnetic H_z field of the TM-mode at a free-space wavelength $1.5 \mu\text{m}$, and (e) the corresponding electric field components E_x and E_y evaluated along the dashed line in (d).

There are fundamental differences between the horizontal- and vertical-stacks. The vertical stack not only offers advantages in fabrication (lower surface roughness) but are also more resilience against high-input powers as plasmonic propagation losses only depend on the distances of the active layer but not the slot width [31]. Differences of the field can be seen by looking at the modal field distributions in different transversal planes of Fig. 1. It is evident, that the modal E -field of the plasmonic mode in the horizontal- and vertical-stack arrangement is parallel respectively perpendicular to the substrate. For efficient coupling of the optical strip waveguide mode by tapering into the plasmonic mode of the modulator, different modes have to be used, namely the TE_{00} (horizontal-stack) and TM_{00} (vertical-stack) modes.

III. PLASMONIC AND PHOTONIC WAVEGUIDES

The plasmonic slot waveguide structure has been introduced in the previous section. Here, we deal with its physics, the propagation of fields and the dispersion relations in plasmonic and photonic waveguides [30], [31].

A. Plasmon Polaritons

Collective oscillations of free electrons within a metallic crystal lattice excited by an external optical radiation lead to the formation of Surface Plasmon Polaritons (SPPs) [32] or Localized Plasmon Polaritons (LPPs) [33]. Both effects describe the coupling of an electromagnetic wave to the free electron gas of a metal and thereby exciting plasmonic oscillations. The quasiparticle of an electromagnetic wave coupled to electrons is then called a polariton. If coupled to a metallic surface it may

propagate along the surface (SPP), if coupled to a small metallic particle the polariton is localized (LPP).

It is instructive to first visualize how a SPP TM-mode propagates over a gold-cladding surface, see Fig. 2. Gold has a complex permittivity (ϵ) with a negative real part over the entire optical and infrared wavelength range, see Fig. 2(b) [34]. The imaginary part of the relative permittivity is also considerable and causes material losses when exposed to an electromagnetic wave.

Simulations have been performed for a SPP TM-mode, at a wavelength of $1.5 \mu\text{m}$. For the simulations we have chosen the measured permittivities of gold, see Fig. 2(b), and a typical organic EO material [35]. To find the propagation constant of the SPP mode one needs to solve the Helmholtz equation at the interface. I.e. one starts by putting down the Ansatz of (1) for the two materials, inserts the Ansatz into the Helmholtz equation and employs the boundary condition at the gold-OEO interface. The dispersion relation for the SPP TM-mode then is [32]

$$\beta_{SPP} = \frac{\omega}{c} \sqrt{\frac{\epsilon_{r1}\epsilon_{r2}}{\epsilon_{r1} + \epsilon_{r2}}}, \quad (2)$$

where ϵ_{r1} and ϵ_{r2} are the relative dielectric permittivities of the coating (EO) and gold, respectively, ω is the angular frequency of the mode, c is the speed of light in vacuum, and β_{SPP} is the complex propagation constant of the SPP. Numerically, one will find the dispersion relation $\beta(\omega)$ of the SPP mode, see Fig. 2(c).

The TM mode of the SPP with field components (H_z, E_x, E_y) has been plotted in Fig. 2(d) and (e).

The amplitude of the wave doesn't visibly decay along the propagation path due to the low imaginary part of the

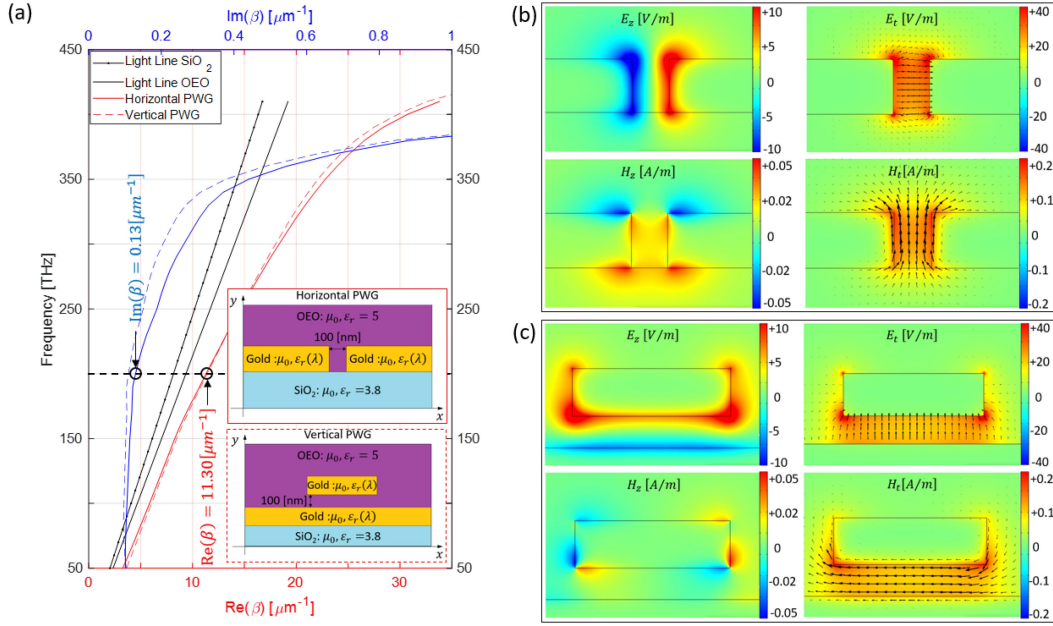


Fig. 3. Dispersion relations and field distributions of horizontal- and vertical-stack plasmonic waveguides (PWG). (a) Waveguide cross-sections and dispersion relations. Fields of guided modes of (b) horizontal and (c) vertical stack plasmonic structure for a free-space wavelength $\lambda = 1.5 \mu\text{m}$. Here, E_z is the z-component of the electric field, \vec{E}_t is the transversal electric field vector, H_z is the z-component of the magnetic field, \vec{H}_t is the transversal component of the magnetic field, $\beta = \text{Re}(\beta) + j\text{Im}(\beta) = \beta_r + j\beta_i$ is the complex propagation constant of the plasmonic waveguide, and OEO represents the chosen organic electro-optical material between the golden electrodes.

propagation constant (2) ($\beta_{SPP} = 8.9 + j0.02 \mu\text{m}^{-1}$) representing the material losses in gold.

Fig. 2(e) shows also the importance of the SPP TM-mode for the field enhancement purposes as the electric field has a pronounced normal component (in this case E_y) which is essential for the field enhancement purposes.

B. Plasmonic Waveguides

Similar as above one can solve the Helmholtz equation for the plasmonic slot waveguides presented in the inset of Fig. 3(a). The slot waveguide is placed on a substrate (SiO_2). Two thin metallic electrodes form the plasmonic waveguide. Within the slot is an EO material. For the given geometry of the waveguides, see Fig. 3(a), a vector FEM eigenvalue analysis [36] has been performed and the corresponding dispersion relation and Eigenfields are presented in Fig. 3(a)–(c).

The dispersion relations in Fig. 3(a) reveal the following important information: (i) The odd plasmonic mode that guarantees the field enhancement in the gap has no cutoff within the desired optical frequency range (which means, that the mode in the slot can be squeezed to any small size limited only by the dielectric breakdown voltage); (ii) The propagation constant of the plasmonic mode is a complex number. Its real part gives an idea on the SPP wavelength

$$\lambda_{SPP} = \frac{2\pi}{\text{Re}(\beta_{SPP})}. \quad (3)$$

From Fig. 3(a) it can be seen that the SPP wavelength is smaller than a photonic wavelength. (iii) The imaginary part represents the plasmonic losses. A decay to $1/e$ of its intensity

is given by

$$L_{1/e} = \frac{1}{\text{Im}(\beta_{SPP})}. \quad (4)$$

The plasmonic losses increase with higher optical frequencies; and (iv) The vertical-stack waveguide (dashed) offers a somewhat lower propagation losses than the horizontal-stack waveguide (solid).

Fig. 3(b) and (c) show the electric and magnetic field of the fundamental plasmonic modes of the horizontal and vertical structures, respectively.

The ideal geometry of a plasmonic waveguide [30] needs to be found by means of extensive simulations. It needs to be designed as a compromise between mutually conflicting requirements, such as maximization of the field interaction between electrical and optical fields, and minimization of the propagation losses and strength of the nonlinear materials in thin films [35]. But, it is also impacted by the slot-etching capabilities of the available manufacturing equipment, etc.

C. Photonic Waveguides

The optical wave is usually launched into a plasmonic waveguide through a tapering section, as depicted in Fig. 4. The photonic waveguide is considerably larger than the plasmonic waveguide. Its dispersion diagrams of the TM_{00} and TE_{00} modes are calculated by using a similar vector FEM eigenvalue solver, as in the previous case of plasmonic waveguide. The curves presented in Fig. 4(b) reveal the cutoff frequencies of the guiding modes that are obtained as a crossing point of the SiO_2 light line and the modal dispersion curve, which practically means that

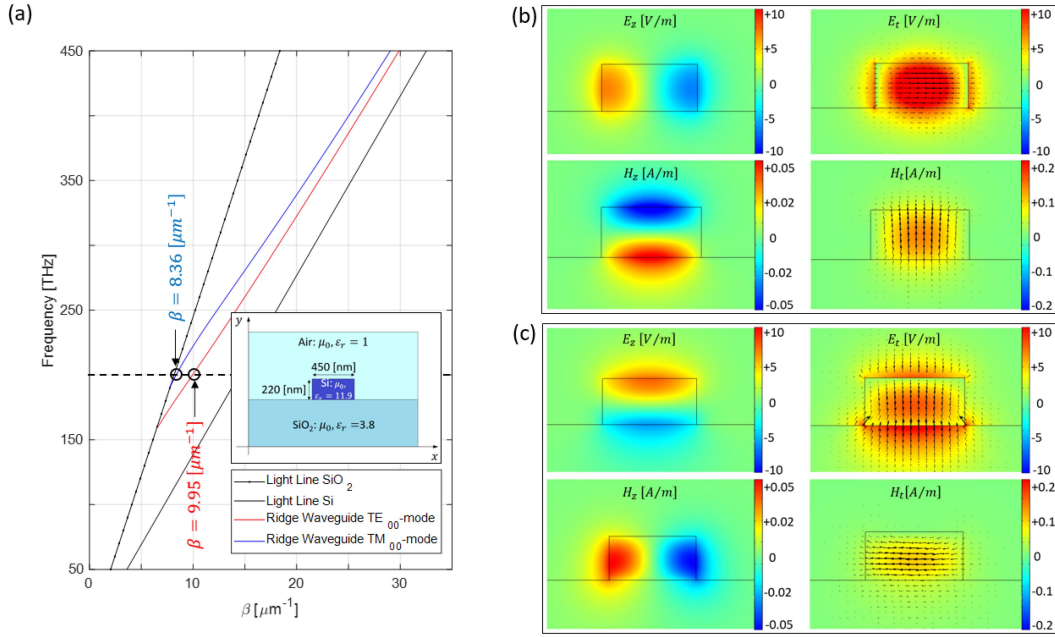


Fig. 4. Dispersion relations and field distributions of photonic waveguide. (a) Waveguide cross-section and dispersion relation of the TE₀₀ and TM₀₀ waveguide mode. (b) Transversal and longitudinal E- and H-fields of the TE₀₀ mode, and (c) transversal and longitudinal E- and H-fields of the TM₀₀ mode, both being computed at the free-space wavelength $\lambda = 1.5 \mu\text{m}$. The cutoff frequency of the TE₀₀ mode is slightly above 150 THz and of the TM₀₀ mode slightly below 200 THz. The cutoff information is essential for choosing the optical frequency range of the modulator.

TABLE I

(ADAPTED FROM [15] AND [43]) PERFORMANCE OF OEO MATERIALS IN POH MODULATORS

Material	Year	r_{33} [pm/V]	T_g [°C]
BAH13 (thin-film)	2022	208	90
JRD1 (thin-film)	2022	123	82
BAH13 (bulk)	2022	620	66
JRD1 (bulk)	2022	560	82
PerkinamineTM (thin-film) [43]	2024	180	170

T_g is the glass transition temperature of the material

TABLE II

(ADAPTED FROM [41], AND [42]) PERFORMANCE OF BTO AND LN THIN FILMS

Material	Year	r_{eff} [pm/V]	r_{42} [pm/V]
Barium Titanate (BTO) at 100 MHz	2023	318	1030
Barium Titanate (BTO) at 100 GHz	2023	231	390
Lithium Niobate (LN)	2023	27	-

r_{eff} results as reported in [42]

r_{42} results as reported in [41] and [42]

below the cutoff frequency the optical wave leaks out of the rectangular Si-core into the substrate. Thus, photonic waveguides have a cutoff frequency and with this also a minimum dimension in contrast to plasmonic waveguides.

It is important also to explain the need for computing both the TE₀₀ and TM₀₀ modes. First of all, the names TE and TM are not properly used in this context due to the fact that the guiding modes are hybrid, i.e., they do have longitudinal E_z and H_z field components, as shown in Fig. 4(b) and (c). However, Fig. 4(b) shows that the maximum of the E_z -field is four times lower than the corresponding maximum of the transversal E_t -field. A similar ratio can be observed also between the H_z -field and H_t -field in Fig. 4(c). The said dominance of the transversal- over longitudinal fields, justifies the widely used TE and TM naming convention.

Secondly, the TE₀₀ mode has the transversal field E_t polarized in the horizontal direction. This is similar to the distribution of the transversal field of the plasmonic waveguide shown in Fig. 3(b). This enables the mode coupling from the photonic into the plasmonic waveguide. A similar logic can be applied to

the TM₀₀ mode with its transversal E_t component being polarized vertically similar to the vertical-stack waveguide shown in Fig. 3(c).

D. Photonic-to-Plasmonic and Plasmonic-to-Photonic Converter

In addition to the radically different geometrical dimensions of the photonic and plasmonic waveguide, the dispersion diagrams shown in Fig. 4(a) and 3(a) reveal considerable differences in the propagation constants of the modes. The geometrical and propagation constant difference require tapering regions for an adjustment of the propagation constants and a smooth modal transition from the large photonic to a much smaller plasmonic mode. This is on its own, a very difficult task that must be carried out by means of 3D electromagnetic simulations.

The tapering section before and after the modulator must be optimized in such a way that the transmission coefficient between the input and output ridge waveguide (measured by the S-parameter S_{21}) is maximized, or, in other words, that the insertion loss of the modulator is minimized.

For solving the said problem, the following procedure can be applied. A 3D electromagnetic simulation model including short sections of the photonic and plasmonic waveguide along with a tapering region in between should be used. Several geometrical parameters should be varied, such as tapering length, order of tapering transition (linear, quadratic, etc.), height, etc. The simulation model should be coupled with a deterministic or stochastic optimization algorithm for governing the improvement in such a way that an optimal solution with lowest insertion loss within the variable limits is found [37].

Several examples of simulation based design of the tapering region between the photonic and plasmonic waveguides exists in the literature, such as for example the papers [38], [39], [40].

IV. MODULATOR FEATURES AND FIGURES OF MERIT

A. Electro-Optical Materials

The refractive index change of a Pockels material is related to an induced electric field E^Ω by [30]

$$\Delta n_{mat} \approx -\frac{1}{2} n_{mat}^3 r_{eff} E^\Omega \quad (5)$$

where n_{mat} is the refractive index of the material, r_{eff} is the ‘‘effective’’ Pockels coefficient, and E^Ω is the external electric field.

It is important to mention that electro-optical materials are usually anisotropic. The Pockels coefficient therefore has the form of a Pockels EO tensor r_{ijk} in a 3D coordinate system of the material’s crystal lattice. And as a matter of fact the overall refractive index change along an axis i due to a field along the axis E_j^ω may consist of multiple contributions from the RF electrical fields along the direction E_k^Ω [30]

$$\Delta n_{ij} = \sum_{k=1}^3 \frac{n_i^2 n_j^2}{n_i + n_j} E_k^\Omega \quad (6)$$

Thus, depending on the orientation of the material in the active region of the modulator, we have an average statistical behavior of different material domains described by the effective Pockels coefficient r_{eff} in (5).

For OEO materials, the effective Pockels coefficient can be very well approximated as $r_{eff} = r_{333}$ because this element is dominant in the Pockels EO tensor. For comparison, the values of the Pockels coefficients of different OEO materials are given in Tabel I, adapted from [24].

Contrary to OEO materials, ferroelectric materials such as BTO have no a dominant component of the Pockels tensor. It is therefore not surprising that r_{eff} depends on the crystalline orientation and direction of both E^Ω and E^ω . Often the crystalline c-axis of BTO is maximized by choosing the waveguide 45° off against the optical field-axis leading to a more complicated relation [19]

$$r_{eff} = \frac{1}{2\sqrt{2}} (r_{113} + r_{333} + 2r_{232}). \quad (7)$$

The BTO Pockels coefficient has recently been measured with respect to its frequency [41], [42]. These measurements revealed quite a frequency dependence for its largest r_{42} component.

Those results are presented in Table II. For the reference, the measured value of Lithium Niobate (LiNbO_3) used in the commercially available modulators is also presented. It is evident that LN lags considerably behind both the OEO materials and BTO.

The OEO materials have been tested for operation at cryogenic temperatures [44] as well for operation at elevated temperatures. OEO materials have been tested for long term operation at 85 °C [23]. The company Polariton Inc., that sells these modulators, has performed long term stability tests. They report in [45] a continuous modulation for 5 hours at 85 °C and 100 GBd NRZ and reliable operation for 6 months at room temperature. At cyrogenic temperatures the OEO materials shows an electro-optic coefficient that is reduced by about 10%. An interesting characteristic of the OEO material is that its temperature coefficient has the opposite sign of silicon. This results in a stable operation of resonant structures such as ring modulators when the temperature of the rings changes [23]. The BTO plasmonic modulators have been operated at 130 °C and no degradation has been found [19]. They have further been exposed to temperatures up to 250 °C and no degradation was found when removing them from the oven [19]. Photonic BTO modulators have also been tested for operation at cryogenic temperatures. They have shown to operate at temperatures of 4K. The effective electro-optical coefficient though drops to below 200 pm/V at dc voltages.

B. Plasmonic Modulator Configurations

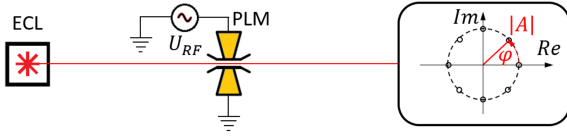
The simplest possible arrangement utilizing the described plasmonic modulator is shown in Fig. 5(a). This is a **phase shifter** [46]. It encodes a phase modulation onto a signal in the complex constellation plane. The effect of the RF-signal is visible in the optical spectrum showing the optical carrier (f_ω) and the side bands ($f_\omega \pm f_\Omega$).

To achieve amplitude modulation instead of phase modulation, one combines two phase shifters into a **Mach-Zehnder modulator (MZM)**, see Fig. 5(b). The voltage sources U_1 and $-U_1$ (push-pull operation mode) are then used for imprinting the RF signal onto the optical carrier in the two arms. In this operation mode the MZM provides a chirp-free amplitude modulation. To fine tune the phase between the optical paths on the arms one may apply an offset DC-bias to the voltage sources or add offset phase-shifters in the arms. In plasmonics such MZM can be as compact as 10 μm in length (including the 1x2 combiner, the photonic-to-plasmonic converters, the plasmonic phase-shifters and the 2x1 splitter) [19]. Already early MZM were operated at 120 Gbit/s with an estimated energy consumption of only 860 aJoule/bit [47].

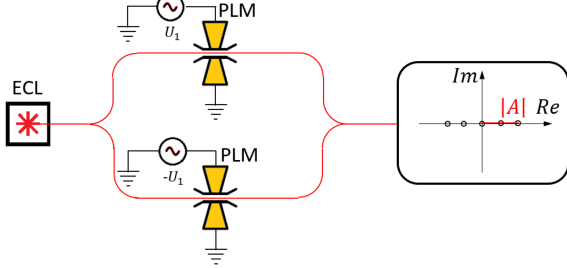
Plasmonic MZMs have been tested for their performance with both organic and inorganic BTO materials. Thereby record transmission rates of 205 GBd and line-rates of 432 Gbit/s have been reported for PAM-8 modulation with plasmonic-organic hybrid modulators, [48]. For plasmonic BTO modulators we recently reported 216 GBd for PAM-2 modulation in Ref. [27], see Fig. 6(a) and 256 GBd in Ref. [49].

Also **plasmonic IQ modulators** have been implemented. This way one can encode advanced modulation formats at

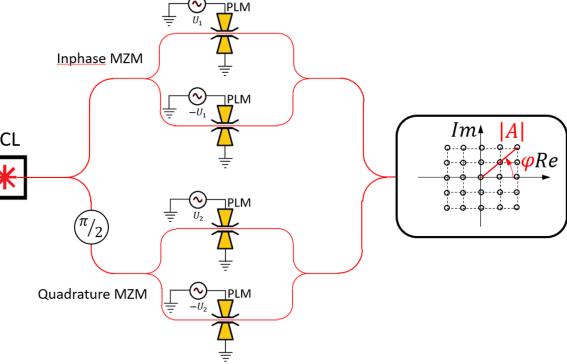
(a) Phase Shifter



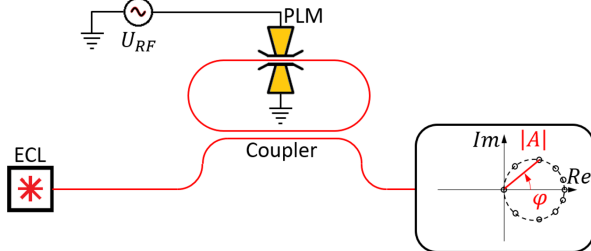
(b) Mach-Zehnder Modulator (MZM)



(c) IQ Modulator



(d) Plasmonic Racetrack Modulator



(e) Plasmonic Ring-assisted MZM

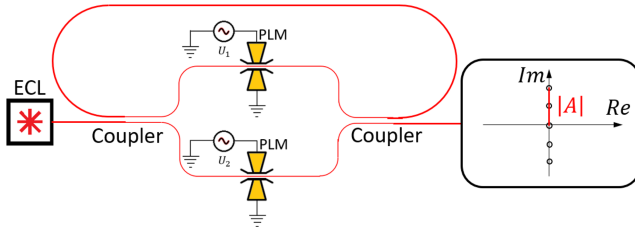


Fig. 5. Different plasmonic modulator (PLM) configurations: (a) Phase shifter arrangement including an external cavity laser (ECL) with PLM and a display of a possible constellation; (b) Mach-Zehnder modulator (MZM); (c) IQ modulator capable of encoding complex modulation; (d) Plasmonic race-track modulator; and (e) plasmonic ring-assisted MZM.

TABLE III
(ADAPTED FROM [22]) PERFORMANCE OF DRIVERLESS PLASMONIC IQ MODULATOR

Data Rate [Gb/s]	Symbol Rate & Modulation	Peak-to-peak Driving Voltage [V]	Energy Consumption [fJ/bit]
50	50 GBd 4QAM	0.145	0.07
200	50 GBd 16QAM	0.567	0.30
400	100 GBd 4QAM	1.480	2.00

The optical on-chip losses: 11-15 dB, operation up to 75°C [22].

highest symbol rates. For an IQ modulator one combines two MZMs. The first MZM provides the encoding of the inphase (I) signal and the 2nd MZM, which if offset by a $\pi/2$ -phase shift provides the quadrature (Q) phase encoding, see Fig. 5(c). The various offset-phase shifters within the configuration are used to optimally adjust the operating points of the MZMs. IQ modulators are needed to encode information in the complex constellation plane.

As an example plasmonic IQ modulators 400 Gb/s 16 QAM signals have been encoded at 100 GBd [22]. Even for such high data rates the power consumption was as small as 2 fJ/bit when operating the device with a peak-to-peak driving RF voltage of 1.48 V measured by a 50 Ω oscilloscope. When encoding 50 Gbit/s by a 4 QAM at 25 GBd the power consumption dropped to as little as 70 aJoule/bit. The required peak-to-peak voltage was as low as 0.145 V. A summary of the performance of the IQ modulator with an organic active electro-optical material as demonstrated in Ref. [22] is presented in Table III. It should be stressed, that peak-voltages below 1 V enable driverless operation.

Rather than MZM modulators one may deploy **ring modulators** [21], [23]. The resonant configuration enables operation with even lower power consumption as one may modulate the signals at an operation point with a steeper transfer function. Also, one can operate them with lower losses as a fraction of the signal can “bypass” the plasmonic ring [21], [50]. Ring modulators are accompanied by a chirp during operation. I.e. when modulating the amplitude one also modulates the phase. The symbols are then not symmetrically distributed in complex space, see Fig. 5(d). Ring modulators are however ideal for on-off keying and PAM operation.

In a recent implementation an undercoupled racetrack modulator was implemented, Fig. 6(d). With this device unprecedented low on-chip device loss of -1.2 dB was shown and operation of 220 Gbit/s 2PAM and 408 Gbit/s 8 PAM was demonstrated [23]. Operation at 408 Gbit/s was performed with as little as 12 fJ/bit and a peak-to-peak voltage of 1.2 V. Additionally, high thermal stability was shown as the permittivity of the silicon waveguides and the plasmonic section featured opposite temperature coefficients [23].

Variations to these configurations exist. For instance, it was shown that a MZM can be complemented by a resonant ring to further increase the steepness of the transfer function and to further reduce the required voltage [51]. In this so-called **ring assisted MZM**, presented in Fig. 5(e), 220 Gbit/s 2PAM

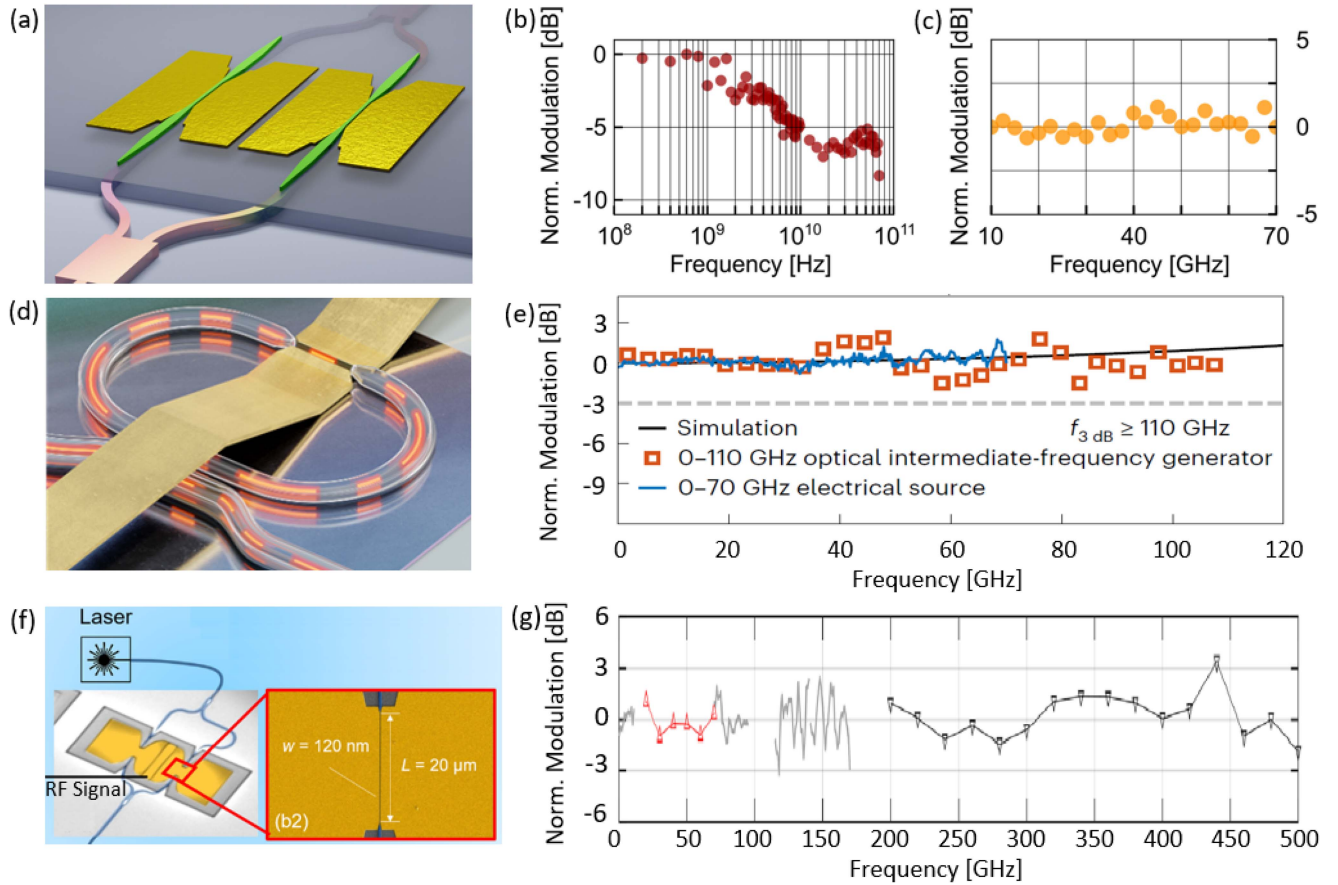


Fig. 6. Examples of fabricated plasmonic electro-optical modulators: (a) Plasmonic Mach-Zehnder modulator fabricated on the silicon nitride (SiN) platform comprising BTO (green) as the active material between electrodes (yellow). Encoding of 256 Gbd data was already demonstrated [27], [49]; (b) and (c) Frequency response of BTO MZM. The BTO electro-optic coefficient drops between 1 and 10 GHz, see [42]; (d) Plasmonic racetrack modulator fabricated on the silicon-insulator platform comprising an organic electro-optical material in the active area. Operation up to 408 Gbit/s with as little as 0.6 V_p has recently been demonstrated [23]; (e) The frequency response of the plasmonic organic hybrid ring modulator; (f) Plasmonic organic MZM with (g) a flat frequency response (beyond 500 GHz) as presented in [4].

modulations were shown with as little as 1.0 V peak-to-peak voltage [52].

C. Modulator Figures of Merit

To gain better insights into the efficiency of modulators and their relevant parameters we move on to the important modulator figures of merit.

The phase shift accumulated by an optical signal when passing along a modulator with an effective refractive index n_{eff} is given by

$$\Delta\varphi = \Delta\beta \cdot L = k_0 \Delta n_{eff} L \quad (8)$$

where $\Delta\beta$ is the change of the propagation constant, associated to the change of the effective group refractive index change $\Delta n_{eff,g}$, k_0 the vacuum wavenumber, and L the modulator length.

By comparing (8) against (5), a very important question arises. What is relation between the effective group refractive index change Δn_{eff} due to the RF modulating field \vec{E}^Ω and its corresponding material index change Δn_{mat} .

The value of Δn_{eff} depends on the material refractive index change Δn_{mat} as given by the applied electric field but also on the interaction between the optical field and electrical field in the active section. This can be expressed by an **interaction factor** [30]

$$\Delta n_{eff} = \Delta n_{mat} \cdot \Gamma \quad (9)$$

whereby its value can be given by [30]

$$\Gamma \approx \frac{\frac{d}{U_{RF}} \frac{1}{Z^\omega} \iint_{(A_m)} E_x^\Omega |E_x^\omega|^2 dx dy}{\iint_{(A_{tot})} \text{Re}(\vec{E}^\omega \times \vec{H}^{\omega*}) \cdot \vec{e}_z dx dy}. \quad (10)$$

The numerator in (8) represents the overlap of the RF-field with the optical power. Here, A_m is the modulator active cross section area, A_{tot} the area through which the optical wave propagates, $Z^\omega = Z_0/n_{mat}$ is the wave impedance of the optical field in the modulator material. It normalizes the optical field E_x^ω in the numerator to a power. The term U_{RF}/d with d being the modulator gap thickness, normalizes the RF field E_x^Ω in the numerator across the plasmonic slot. The denominator normalizes the optical power of the plasmonic mode. The plot in Fig. 7(a) gives an idea on the interaction factor as a function

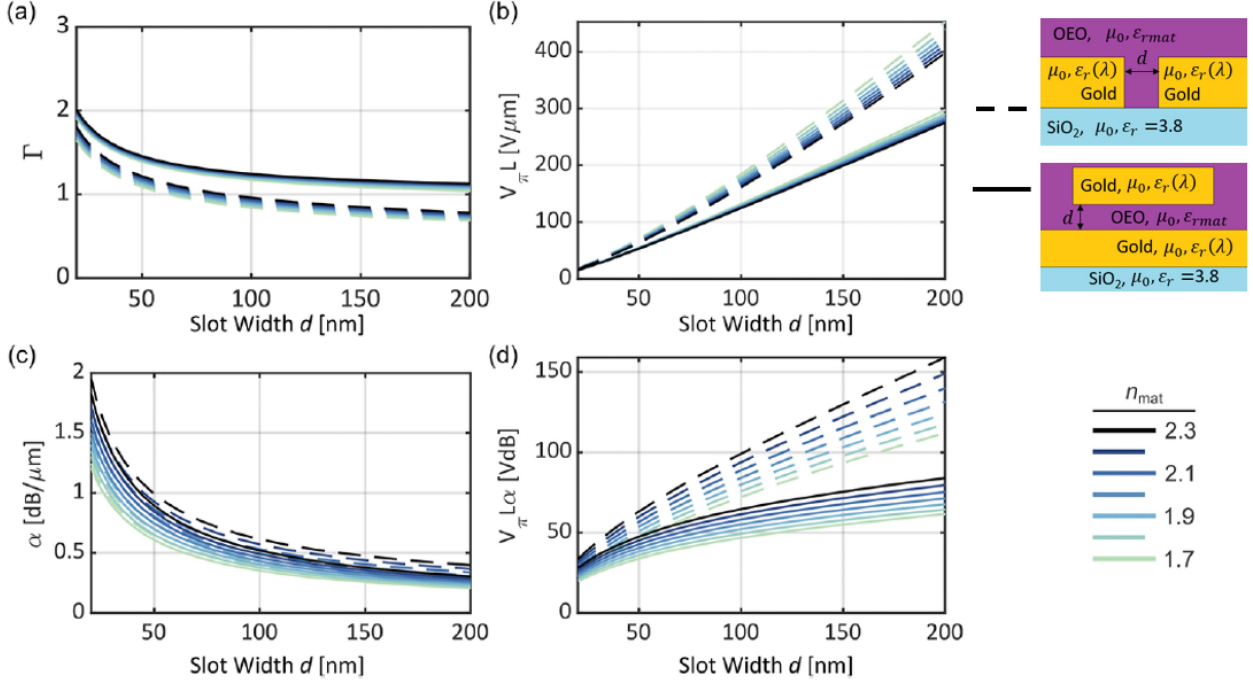


Fig. 7. Important modulator figures of merit of a plasmonic phase shifter for a horizontal (dashed) and vertical (solid) plasmonic stack. Calculations are shown as a function of the slot width for different active materials with refractive indices n_{mat} varying between 1.7 and 2.3. The plots show (a) the field interaction factor, (b) the modulation efficiency in terms of the $V_{\pi}L$ figure of merit, (c) α the loss per micrometer, and (d) the combined $V_{\pi}L\alpha$ figure of merit (adopted from [30]).

of slot width, refractive index of the active material (lines with different colors) and the geometry (horizontal slots are dashed, vertical slots are solid). Having (10), it is possible to combine (5) with (8)–(10) in order to obtain the following important equation

$$\Delta\varphi \approx \frac{1}{2}k_0n_{mat}^3r_{eff}\frac{U_{RF}}{d}\Gamma L \quad (11)$$

Equation (11) is relevant to derive the modulator's **figure of merit** $V_{\pi}L$ (often called **modulation efficiency**)

$$V_{\pi}L \approx \frac{2\pi d}{k_0n_{mat}^3r_{eff}\Gamma} = \frac{\lambda d}{n_{mat}^3r_{eff}\Gamma} \quad (12)$$

where λ is the free-space optical wavelength and V_{π} is the voltage U_{RF} of the RF signal required for reaching a phase shift $\Delta\varphi = \pi$. Since length can be traded in for V_{π} this is indeed a useful figure of merit. From the plot in Fig. 7(b) one can see that keeping the slot width small results in lower $V_{\pi}L$.

In addition to the modulation efficiency (12), the **loss factor** $\alpha = \beta_i$ along the plasmonic waveguide is another important figure of merit

$$\vec{E}_t^{\omega}(\vec{r}_t, L) = \vec{E}_t^{\omega}(\vec{r}_t, 0)e^{-\alpha L}e^{j\beta_r(\vec{E}^{\omega})L}, \quad (13)$$

where the complex propagation constant of the plasmonic waveguide is rewritten by $\beta_{PWG} = \beta_r + j\alpha$. The plots in Fig. 7(c) show that losses increase with smaller slot widths. The loss factor is sometimes combined with the modulation efficiency forming the **$V_{\pi}L\alpha$ value**, as shown in Fig. 7(d).

Applying the above figures of merit to electromagnetic field simulations, one obtains the interesting results in Fig. 7, [30]. Here, vertical (solid lines) and horizontal (dashed lines) plasmonic stacks were compared against each other with respect to

the slot width as a parameter. Fig. 7(a) shows how reducing the slot width leads to a higher field interaction factor Γ . According to (12) this should yield lower $V_{\pi}L$. And indeed, $V_{\pi}L$ can become as small as 100 $V\mu m$, Fig. 7(b). The loss factor α , however, is increased with smaller slot widths, as visible in Fig. 7(c). This is expected, because higher field confinement means higher plasmonic losses in gold due to its complex dielectric permittivity. And despite of the increased losses, the overall performance captured by the $V_{\pi}L\alpha$ shows that smaller slot widths provide better performances, Fig. 7(d).

This result has been experimentally confirmed in [35], where the device with the slot width of 70 nm has the best performance in the experiment. However, going to even smaller slot width seems unrealistic to fabricate and results in worse efficiencies due to surface effects [35]. Someone could think that smaller slot widths could lead to higher capacitances which could reduce the frequency limit of the modulator due to its low-pass ($1/RC$) frequency characteristic. However, this is not a problem, since the device has an extremely small length and height, still having a flat frequency response up to at least 500 GHz [4].

Fig. 7 also shows evidently that the vertical stack arrangement outperforms its horizontal counterpart in all their variants. This can be explained by lower confinement of the optical field in the larger slot space having the same confinement of the RF-field determined only by the slot width. This is why the vertical stack is more appropriate for high optical power applications.

The presented theoretical and simulation results are validated multiple times by comparison against measurements and a very good agreement was found. For instance, in Ref. [19] we report a plasmonic modulator with $V_{\pi}L$ values as low as 60 $V\mu m$. Considering the complexity of fabrication and measurements

on one side and uncertainties in modeling and simulation on the other side the reported values may be considered a good match with the simulation in Fig. 7(d).

D. Modulator Optimization

The goal of a modulator design is to minimize the aforementioned $V_\pi L$ value. Equation (12) shows that $V_\pi L$ can be minimized by (a) transitioning to materials with a higher Pockels effect (which is obtained in plasmonics by the choice of organic electro-optical materials and ferroelectric materials with a high Pockels coefficient); (b) Designing the plasmonic waveguide with the smallest possible slot d , which is achieved in plasmonics because plasmonic slot waveguides can be minimized as there is no cut-off wavelength. (Plasmonic slots are typically a factor 4 smaller than what is possible with photonics); and (c) Developing the plasmonic waveguide with the highest possible field interaction factor Γ (again, it needs to be stressed that plasmonic interaction factors are a factor 5 to 10 larger than photonic interaction factors).

At this point the authors would like to stress that the V_π is an ambiguous figure of merit. It would be better to specify the required on-off voltage of a device. So, for instance, Mach-Zehnder modulators are usually driven in the push-pull operation mode. There, opposite voltages are applied over each arm, resulting in $V_{\text{on/off}} = 1/2 \cdot V_\pi$. Further, when using plasmonic modulators, which can be treated as lumped, open circuit capacitors without a 50Ω termination, one benefits from another factor 2, see Ref. [14]. Also, driving the lumped elements in a differential way adds another factor of 2, see Ref. [47]. If all these design and optimization tricks are used one can modulate a MZM from on-to-off by as little as $V_{\text{on/off}} = 1/8 \cdot V_\pi$ [47]. And indeed in said Ref. [47] we report operation of plasmonic MZMs with peak-to-peak voltages V_{pp} as little as 0.178 V in a 120 Gbit/s PAM2 experiment. The required swing of a CMOS circuit then as a matter of fact is only half as large, i.e., $V_p = 89$ mV. The power consumption was calculated to be as small as 862 aJ/bit.

E. Frequency Response

The frequency response of a modulator depends on multiple factors. They are material related but also depend on the configuration.

First, the electro-optical coefficient – the Pockels coefficient – is frequency dependent. At lower frequencies and up to a tens of MHz it is dominated by the piezoelectric effect and lattice vibrations related to acoustic phonons. At higher frequencies the ionic movements dominate (optical phonons) contributions dominate. They might contribute up to a few THz. The highest frequency components are typically due to electronic resonances which have contributions up to the PHz. Organic materials owe their nonlinearity mainly to the electronic contributions. They therefore offer some of the largest frequency responses up to highest speed. Ferroelectric materials typically owe the nonlinearity to ionic resonances.

Second, the frequency response depends on the configuration. Normal modulators with travelling wave electrodes are normally

limited by the walk-off between optical and electrical wave. Plasmonic modulators are RC-limited.

The plot in Fig. 6(b) and (c) show the frequency response of a BTO plasmonic modulator. The frequency response between 1 and 10 GHz is an inherent drop and is BOT material related (drop of ionic movements). Afterwards the response remains flat up to at least 100 GHz.

The plot in Fig. 6(e) show the frequency response of a plasmonic organic modulator. Its response remains flat up to and beyond 500 GHz.

F. Implementation Examples

Plasmonic modulators can be implemented on a wide range of platforms with a wide range of Pockels materials. They can be implemented as plasmonic BTO modulators (Fig. 6(a), [19]) or plasmonic organic modulators (Fig. 6(d), [23]). They have been implemented in Mach-Zehnder, IQ-modulator, ring or ring-assisted modulator configurations. We now leave this classical modulator implementations and rather focus on plasmonic modulator implementations that are unique to the plasmonic technologies and that would be difficult – if not impossible to be implemented in any other technology.

Ultra-dense modulator arrays: In Ref. [53], plasmonic modulators were arranged at a pitch of $24 \mu\text{m}$. This way they have been delivering 0.8 Tbit/s on an ultra-compact $90 \mu\text{m} \times 5.5 \mu\text{m}$ footprint. As shown in Fig. 8(a), this solution enables coupling of modulated light into a multi-core fiber. The solution required circular gratings for directing the optical radiation from and into a multi-core fiber and straight into the plasmonic modulator [53].

All-metallic Plasmonic Modulator: (to be stacked on a CMOS chip): Fig. 8(b) features another interesting example, by following [54]. This shows that by going to an all-metallic plasmonic modulator technology one can fabricate the modulators on any substrate. The all-metallic device encompasses vertical grating couplers, splitters, polarization rotators and active phase shifters in a single metal layer. Light is coupled in and out through a multicore optical fiber [54]. An organic electro-optical Pockels-material has been used. This technology was later on used to directly fabricate plasmonic modulators on a BiCMOS chip [56]. Thereby the electrical high-speed signals could be passed on through vias from the electronic to the plasmonic layers stack. This way the first monolithic 180 Gbit/s electronic-plasmonic photonic could be demonstrated [57]. It so far remains the most fast electronic-photonic PIC.

Plasmonic RF-to-Optical Antenna: Last but not least, it is possible to combine a plasmonic modulator and a mm-wave antenna with a pronounced field enhancement capabilities, as presented in [58], [55]. This enables future field sensors capable of detecting and measuring RF waves up to highest frequencies. A first 2.5 THz sensor has already been demonstrated [5].

G. Fabrication

Details on the fabrication of the various implementations have been given in the respective publications. Here, we can outline the general fabrication steps for the sake of completeness.

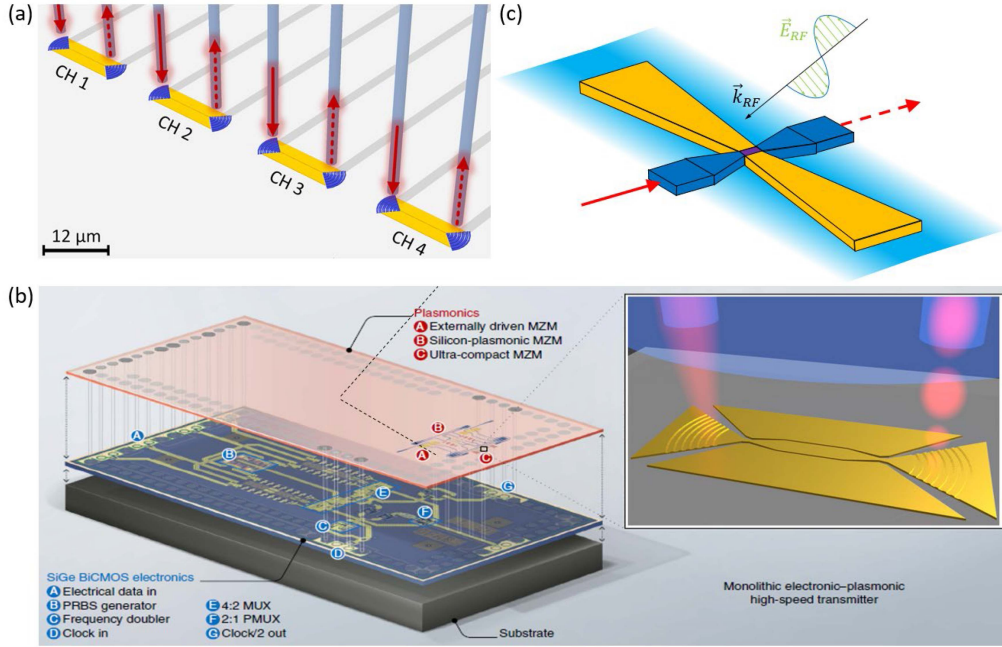


Fig. 8. Advanced implementation examples of plasmonic modulators. (a) 4-channel plasmonic modulator array. Modulators were arranged at a pitch of $24 \mu\text{m}$. Operation at $4 \times 200 \text{ Gbit/s}$ was shown [53]; (b) Plasmonic modulator monolithically integrated on top of BiCMOS layer stack. This way 180 Gbit/s on-chip modulation was demonstrated in single chip [57]. The plasmonic modulator built by a single metal layer is shown as an inset [54]. (c) Plasmonic modulator embedded into the slot of a bow-tie antenna for sensing RF fields up to 500 GHz [55] and even 2.4 THz [5].

Fabrication of the plasmonic organic hybrid (POH) devices [19] is performed on traditional silicon photonic wafers. In a first steps the silicon waveguides are defined. Subsequently, the plasmonic gold waveguides and electrode pads are defined by means of electron beam lithography (EBL). Given that plasmonic waveguides have dimensions in the order of 100 nm the lithographic features size needs to be in the order of $10\text{--}20 \text{ nm}$. Subsequently, the electro-optical material is spin-coated onto the wafer [1]. In a last step the electro-optical material needs to be poled by applying a voltage between the electrodes of the modulators at an elevated temperature.

Fabrication of the BTO plasmonic waveguides in Si [20] or SiN [27] typically starts by implementing conventional Si or SiN waveguides within the respective platform. After an oxide cladding the respective waveguide wafers are planarized and the ferroelectric material is bonded. Then, the BTO is patterned with EBL and etched to form the waveguides. In a next step, the metal is deposited to form the plasmonic modulator.

H. Comparisons of Modulator Technologies

The capabilities and potential of plasmonic EO modulators can be clearly seen when comparing different modulator types against the available competing technologies.

In Table IV we compare different MZ type modulators. Among which are photonic, plasmonic and hybrid plasmonic modulators. The table shows the advantages of plasmonic EO modulators. Plasmonic EO modulators offer (a) an order of magnitude higher modulation efficiency and consequently lower $V_{\pi}L$ values, (b) miniature length and subwavelength cross sections, (c) unmatched frequency and bandwidths unreachable to

TABLE IV
(ADAPTED FROM [30]) TYPICAL MEASURED PERFORMANCE OF EO MZM MODULATORS

Modulator Variant	$V_{\pi}L$ [V μm]	$V_{\pi}L\alpha$ [VdB]	Length L [μm]	on-chip loss α [dB]	Bandwidth [GHz]
SOI [59]	600	1.2	2'000	5.4	60
SOH [60] [17]	400	1.0	280	2.2 ^{1,2}	100
LNOI [61]	22'000	2.2	5'000	1.5	100
BaTiO ₃ [62] ³	4'800	4.8	2'000	2	50
HS PLM [19] [63]	60	30	10	6	>500
VS PLM [31]	100	50	11	5.5	>300
Hybrid PL [25]	350	87	10	2.5	>270

SOI = Silicon on Insulator photonic modulator

SOH = Silicon Organic Hybrid photonic modulator

LNOI = Lithium Niobate on Insulator photonic modulator

BaTiO₃ = BTO photonic modulator

HS PLM = Horizontal Stack Plasmonic Modulator

VS PLM = Vertical Stack Plasmonic Modulator

Hybrid PL = Hybrid Plasmonic Modulators (i.e. only one metal electrode)

¹With 200 V gate voltage to create electron accumulation layer

²On-chip losses based on stated MMI, stop-to-slot converter and phase-shifter losses.

³Some data have been estimated from the published results for obtaining consistent data.

any other existing modulator technology. (d) Plasmonic modulators have higher losses. Yet, there is at worst a 3 dB penalty and latest hybrid plasmonic modulators promise losses comparable to other technologies while bandwidths are still large.

Table V shows the parameters and performance of resonant ring modulators. It is evident that plasmonic modulators also outperform their traditional resonant counterparts in terms of

TABLE V
PERFORMANCE OF EO RESONANT MODULATORS

Modulator Variant	$V_{\pi}L$ [V μm]	V_{peak} [V]	C [μm]	Q	α [dB]	BW [GHz]
Si RM [64]	3'700	0.8	31	4'800	4	45
Si RT [65]	8'000	*	60	5'600	3	67
PLM RM [21]	*	3.3	6	30	2.5	115
PLM RT [23]	150	0.6	90	700	1.2	176

α = on-chip-loss; BW = Bandwidth; C = Ring's Circumference

V_{peak} = driving peak voltage of the experiment

Si RM = Silicon Ring Modulator

Si RT = Silicon Racetrack Modulator

PLM RM = Plasmonic Ring Modulator

PLM RT = Plasmonic Racetrack-Modulator

speed. Due to the high Q-factor they can operate with extremely low driving voltage of 0.6 V for operation up to 200 GBd. Also, it can be seen that plasmonic on-chip losses are extremely low.

V. CONCLUSION

Theory, operational principles, geometrical arrangements, materials and capabilities of plasmonic electro-optical modulators have been presented. Challenges as well as opportunities of this new and emerging technology have been summarized. Recent advancement in terms of design, optimization and fabrication of Pockels effect based plasmonic modulators has revealed their full potential demonstrating the flat frequency response and bandwidth of 500+ GHz, unprecedented level of miniaturization, extremely low power consumption, reliable operation, and thermal robustness and stability.

The main advantages of plasmonic modulators is the ability to overcome the bandwidth and frequency limitations of current photonic modulator technologies. A flat frequency response in excess of 500 GHz has been shown. Operation up to 2.4 THz was demonstrated. In addition, plasmonic modulators offer a most compact footprint enabling the implementation of MZM and ring modulators on footprints as compact as 10 μm^2 , and power consumption of 70 and 300 atto Joules at 50 and 200 Gbit/s. All of which comes at the price of plasmonic losses. Losses that are steadily decreasing as technology matures.

Future developments on plasmonic modulators focus on the implementation of new materials with very pronounced Pockels effect that offer larger nonlinearities at even lower losses. Also, different resonance effects might be exploited in order to further decrease power consumption. An open question is the ultimate bandwidths of the OEO plasmonic modulators. So far a flat frequency response up to 500 GHz was found. Yet it is unclear as of where the response will be dropping off. It will also be decisively important to cointegrate plasmonic modulators with electronics. This way RF losses can be minimized and operation at highest bandwidths can be realized.

Many of the papers cited in this review have come out of research produced within the authors research group. This has not been done by intent, but rather reflects the intense work in this field performed by the group. However, the authors hope that this review helps to inspire other groups to enter this the exciting field of plasmonic modulation.

REFERENCES

- [1] L. R. Dalton et al., "Perspective: Nanophotonic electro-optics enabling THz bandwidths, exceptional modulation and energy efficiencies, and compact device footprints," *APL Mater.*, vol. 11, May 2023, Art. no. 050901, doi: [10.1063/5.0145212](https://doi.org/10.1063/5.0145212).
- [2] A. V. Krishnamoorthy et al., "From chip to cloud: Optical interconnects in engineered systems," *J. Lightw. Technol.*, vol. 35, no. 15, pp. 3103–3115, Aug. 2017.
- [3] C. A. Thraskias et al., "Survey of photonic and plasmonic interconnect technologies for intra-datacenter and high-performance computing communications," *IEEE Commun. Surveys Tuts.*, vol. 20, pp. 2758–2783, Fourthquarter 2018.
- [4] M. Burla et al., "500 GHz plasmonic Mach-Zehnder modulator enabling sub-THz microwave photonics," *APL Photon.*, vol. 4, no. 5, May 2019, Art. no. 056106, doi: [10.1063/1.5086868](https://doi.org/10.1063/1.5086868).
- [5] Y. Salamin et al., "Compact and ultra-efficient broadband plasmonic terahertz field detector," *Nature Commun.*, vol. 10, no. 1, Dec. 2019, Art. no. 5550, doi: [10.1038/s41467-019-13490-x](https://doi.org/10.1038/s41467-019-13490-x).
- [6] G. Sinatkas, T. Christopoulos, O. Tsilipakos, and E. E. Kriezis, "Electro-optic modulation in integrated photonics," *J. Appl. Phys.*, vol. 130, Jul. 2021, Art. no. 010901, doi: [10.1063/5.0048712](https://doi.org/10.1063/5.0048712).
- [7] J. B. Khurgin, V. J. Sorger, and R. Amin, "Charge and field driven integrated optical modulators: Comparative analysis: Opinion," *Opt. Mater. Exp.*, vol. 12, pp. 1784–1789, 2022.
- [8] D. Petousi et al., "Analysis of optical and electrical tradeoffs of traveling-wave depletion-type Si mach-Zehnder modulators for high-speed operation," *IEEE J. Sel. Top. Quantum Electron.*, vol. 21, pp. 199–206, Jul./Aug. 2015, doi: [10.1109/JSTQE.2014.2369516](https://doi.org/10.1109/JSTQE.2014.2369516).
- [9] H. Xu et al., "High-speed silicon modulator with band equalization," *Opt. Lett.*, vol. 39, 2014, Art. no. 4839, doi: [10.1364/OL.39.004839](https://doi.org/10.1364/OL.39.004839).
- [10] P. Dong et al., "224-Gb/s PDM-16-QAM modulator and receiver based on Silicon photonic integrated circuits," in *Proc. IEEE Opt. Fiber Commun. Conf. Fiber Opt. Eng. Conf.*, 2013, Paper PDP5C.6, doi: [10.1364/OFC.2013.PDP5C.6](https://doi.org/10.1364/OFC.2013.PDP5C.6).
- [11] C. H. Henry, R. F. Kazarinov, H. J. Lee, K. J. Orlowsky, and L. E. Katz, "Low loss Si₃N₄-SiO₂ optical waveguides on Si," *Appl. Opt.*, vol. 26, no. 13, pp. 2621–2624, Jul. 1987, doi: [10.1364/AO.26.002621](https://doi.org/10.1364/AO.26.002621).
- [12] S. Abel et al., "A strong electro-active lead-free ferroelectric integrated on silicon," *Nature Commun.*, vol. 4, 2013, Art. no. 1671.
- [13] L. Alloati et al., "42.7 Gbit/s electro-optic modulator in silicon technology," *Opt. Exp.*, vol. 19, pp. 11841–11851, 2011.
- [14] J. Leuthold et al., "Silicon-organic hybrid electro-optical devices," *IEEE J. Sel. Topics Quantum Electron.*, vol. 19, no. 6, Nov./Dec. 2013, Art. no. 3401413.
- [15] H. Xu et al., "Design and synthesis of chromophores with enhanced electro-optic activities in both bulk and plasmonic-organic hybrid devices," *Mater. Horiz.*, vol. 9, pp. 261–270, 2022.
- [16] A. Schwarzenberger et al., "O-band SOH Mach-Zehnder modulator operating at a PAM4 line rate of 384 gbit/s with sub-volt drive voltage," in *Proc. Opt. Fiber Commun. Conf. Exhib.*, 2024, Paper Th4B.6.
- [17] L. Alloati et al., "100 GHz silicon-organic hybrid modulator," *Light Sci. Appl.*, vol. 3, 2014, Art. no. e173, doi: [10.1038/lsa.2014.54](https://doi.org/10.1038/lsa.2014.54).
- [18] C. Wang, M. Zhang, B. Stern, M. Lipson, and M. Lončar, "Nanophotonic lithium niobate electro-optic modulators," *Opt. Exp.*, vol. 26, pp. 1547–1555, 2018.
- [19] C. Haffner et al., "All-plasmonic Mach-Zehnder modulator enabling optical high-speed communication at the microscale," *Nature Photon.*, vol. 9, pp. 525–528, 2015.
- [20] A. Messner et al., "Plasmonic ferroelectric modulators," *J. Lightw. Technol.*, vol. 37, no. 2, pp. 281–290, Jan. 2019, doi: [10.1109/JLT.2018.2881332](https://doi.org/10.1109/JLT.2018.2881332).
- [21] C. Haffner et al., "Low-loss plasmon-assisted electro-optic modulator," *Nature*, vol. 556, pp. 483–486, 2018.
- [22] W. Heni et al., "Plasmonic IQ modulators with attojoule per bit electrical energy consumption," *Nature Commun.*, vol. 10, 2019, Art. no. 1694, doi: [10.1038/s41467-019-09724-7](https://doi.org/10.1038/s41467-019-09724-7).
- [23] M. Eppenberger et al., "Resonant plasmonic micro-racetrack modulators with high bandwidth and high temperature tolerance," *Nature Photon.*, vol. 17, pp. 360–367, 2023.
- [24] C. Haffner et al., "Harnessing nonlinearities near material absorption resonances for reducing losses in plasmonic modulators," *Opt. Mater. Exp.*, vol. 7, pp. 2168–2181, 2017.
- [25] P. Ma et al., "Low-loss plasmonically enhanced graphene-organic hybrid phase modulator with >270 GHz modulation bandwidth," in *Proc. Eur. Conf. Opt. Commun.*, 2022, Paper Th3B.4.

- [26] A. Melikyan et al., “High-speed plasmonic phase modulators,” *Nature Photon.*, vol. 8, pp. 229–233, 2014.
- [27] M. Kohli et al., “Plasmonic ferroelectric modulator monolithically integrated on SiN for 216 Gb/d data transmission,” *J. Lightw. Technol.*, vol. 41, no. 12, pp. 3825–3831, Jun. 2023, doi: [10.1109/JLT.2023.3260064](https://doi.org/10.1109/JLT.2023.3260064).
- [28] M. Thomaschewski, V. A. Zenin, S. Fiedler, C. Wolff, and S. I. Bozhevolnyi, “Plasmonic lithium niobate Mach–Zehnder modulators,” *Nano Lett.*, vol. 22, pp. 6471–6475, 2022.
- [29] T. D. Bucio et al., “Silicon nitride photonics for the near-infrared,” *IEEE J. Sel. Topics Quantum Electron.*, vol. 26, no. 2, Mar./Apr. 2020, Art. no. 8200613, doi: [10.1109/JSTQE.2019.2934127](https://doi.org/10.1109/JSTQE.2019.2934127).
- [30] A. Messner et al., “Plasmonic, photonic, or hybrid? Reviewing waveguide geometries for electro-optic modulators,” *APL Photon.*, vol. 8, 2023, Art. no. 100901, doi: [10.1063/5.0159166](https://doi.org/10.1063/5.0159166).
- [31] A. Messner et al., “Broadband metallic Fiber-to-chip couplers and a low-complexity integrated plasmonic platform,” *Nano Lett.*, vol. 21, pp. 4539–4545, 2021.
- [32] J. Greffet, “Introduction to surface plasmon theory,” in *Plasmonics* (Springer Series in Optical Sciences), S. Enoch and N. Bonod Eds. Berlin, Germany: Springer-Verlag, 2012, ch. 4, pp. 105–148, doi: [10.1007/978-3-642-28079-5_4](https://doi.org/10.1007/978-3-642-28079-5_4).
- [33] A. Dorodnyy, J. Smajic, and J. Leuthold, “Mie scattering for photonic devices,” *Laser Photon. Rev.*, vol. 17, 2023, Art. no. 2300055.
- [34] P. B. Johnson and R. W. Christy, “Optical constants of the noble metals,” *Phys. Rev.*, vol. 6, pp. 4370–4379, Dec. 1972.
- [35] W. Heni et al., “Nonlinearities of organic electro-optic materials in nanoscale slots and implications for the optimum modulator design,” *Opt. Exp.*, vol. 25, pp. 2627–2653, 2017.
- [36] J. Smajic, *How To Perform Electromagnetic Finite Element Analysis*. Hamilton, U.K.: Int. Assoc. Eng. Modelling, Anal. Simul. Community, 2016.
- [37] J. Smajic, Ch. Hafner, and D. Erni, “Optimization of photonic crystals structures,” *J. Opt. Soc. Amer. A*, vol. 21, no. 11, pp. 2223–2232, 2004.
- [38] Y. Song, J. Wang, Q. Li, M. Yan, and M. Qiu, “Broadband coupler between silicon waveguide and hybrid plasmonic waveguide,” *Opt. Exp.*, vol. 18, no. 12, pp. 13173–13179, 2010.
- [39] A. Melikyan et al., “Photonic-to-plasmonic mode converter,” *Opt. Lett.*, vol. 39, pp. 3488–3491, 2014.
- [40] D. Chelladurai et al., “Low-loss hybrid plasmonic coupler,” *Opt. Exp.*, vol. 27, pp. 11862–11868, 2019.
- [41] D. Chelladurai et al., “Pockels coefficients in thin-film barium titanate and lithium niobate up to 300 GHz,” in *Proc. CLEO*, 2023, Paper SM2H.8.
- [42] J. Winiger et al., “PLD epitaxial thin-film BaTiO₃ on MgO – dielectric and electro-optic properties,” *Adv. Mater. Interfaces*, vol. 11, Jan. 2024, Art. no. 2300665, doi: [10.1002/admi.202300665](https://doi.org/10.1002/admi.202300665).
- [43] M. Lebby, “Electro-optic polymers for heterogeneous integration’ by Lightwave Logic; OFC Workshop 2024: ‘will heterogeneous Integration meet the needs of future applications?,” in *Proc. Opt. Fiber Commun. Conf. Exhib.*, 2024, pp. 1–3.
- [44] D. Bisang et al., “Plasmonic modulators in cryogenic environment featuring bandwidth in excess of 100 GHz and reduced Plasmonic losses,” in *Proc. 48th Eur. Conf. Opt. Commun.*, 2022, Paper Tu1G.1.
- [45] C. Hoessbacher et al., “Plasmonic modulators: Bringing a new light to Silicon,” in *Proc. IEEE 49th Eur. Conf. Opt. Commun.*, 2023, pp. 1606–1608.
- [46] A. Melikyan et al., “High-speed plasmonic phase modulators,” *Nature Photon.*, vol. 8, pp. 229–233, 2014, doi: [10.1038/nphoton.2014.9](https://doi.org/10.1038/nphoton.2014.9).
- [47] B. Baeuerle et al., “120 Gb/s plasmonic Mach-Zehnder modulator with Co-designed electronics operating with 89 mVp driving voltages,” *Opt. Exp.*, vol. 27, 2019, Art. no. 16823.
- [48] Q. Hu et al., “Ultrahigh-net-bitrate 363 Gbit/s PAM-8 and 279 Gbit/s poly-binary optical transmission using plasmonic Mach-Zehnder modulator,” *J. Lightw. Technol.*, vol. 40, no. 10, pp. 3338–3346, May 2022.
- [49] M. Kohli et al., “256 Gb/d barium-titanate-on-SiN mach-zehnder modulator,” in *Proc. Opt. Fiber Commun. Conf.*, 2024, Paper M3K.
- [50] T. Blatter et al., “Is there an ideal plasmonic modulator configuration?,” in *Proc. Eur. Conf. Opt. Commun.*, 2022, Paper Tu4E.4.
- [51] T. Ye and X. Cai, “On power consumption of silicon-microring-based optical modulators,” *J. Lightw. Technol.*, vol. 28, no. 11, pp. 1615–1623, Jun. 2010.
- [52] Y. Horst Blatter et al., “Is there an ideal plasmonic modulator configuration?,” in *Proc. Eur. Conf. Opt. Commun.*, 2022, Paper Tu4E.4.
- [53] U. Koch et al., “Ultra-compact terabit plasmonic modulator array,” *J. Lightw. Technol.*, vol. 37, no. 5, pp. 1484–1491, Mar. 2019.
- [54] M. Ayata et al., “High-speed plasmonic modulator in a single metal layer,” *Science*, vol. 358, pp. 630–632, 2017.
- [55] H. Ibili et al., “Modeling plasmonic antennas for the millimeterwave & THz range,” *IEEE J. Sel. Topics Quantum Electron.*, vol. 29, no. 5, Sep./Oct. 2023, Art. no. 8501115, doi: [10.1109/JSTQE.2023.3314696](https://doi.org/10.1109/JSTQE.2023.3314696).
- [56] U. Koch et al., “A monolithic bipolar CMOS electronic-plasmonic high-speed transmitter,” *Nature Electron.*, vol. 3, pp. 338–345, 2020, doi: [10.1038/s41928-020-0417-9](https://doi.org/10.1038/s41928-020-0417-9).
- [57] D. Moor, J. Leuthold, Y. Fedoryshyn, M. Möller, and U. Koch, “Plasmonic transceivers for the Terabaud age,” *IEEE J. Sel. Topics Quantum Electron.*, vol. 30, no. 4, Jul./Aug. 2024, Art. no. 6000211, doi: [10.1109/JSTQE.2023.3298375](https://doi.org/10.1109/JSTQE.2023.3298375).
- [58] Y. Salamin et al., “Direct conversion of free space millimeter waves to optical domain by plasmonic modulator antenna,” *Nano Lett.*, vol. 15, no. 12, pp. 8342–8346, Dec. 2015, doi: [10.1021/acs.nanolett.5b04025](https://doi.org/10.1021/acs.nanolett.5b04025).
- [59] M. Li, L. Wang, X. Li, X. Xiao, and S. Yu, “Silicon intensity Mach-Zehnder modulator for single lane 100 Gb/s applications,” *Photon. Res.*, vol. 6, pp. 109–116, 2018.
- [60] C. Kieninger et al., “Silicon-organic hybrid (SOH) Mach-Zehnder modulators for 100 Gb/d PAM4 signaling with sub-1 dB phase-shifter loss,” *Opt. Exp.*, vol. 28, pp. 24693–24707, 2020.
- [61] C. Wang et al., “Integrated lithium niobate electro-optic modulators operating at CMOS-compatible voltages,” *Nature*, vol. 562, pp. 101–104, 2018.
- [62] W. Li et al., “Thin-film BTO-based MZMs for next-generation IMDD transceivers beyond 200 Gbps/λ,” *J. Lightw. Technol.*, vol. 42, no. 3, pp. 1143–1150, Feb. 2024.
- [63] Y. Horst et al., “Tbit/s line-rate satellite feeder links enabled by coherent modulation and full-adaptive optics,” *Light: Sci. Appl.*, vol. 12, 2023, Art. no. 153.
- [64] Y. Ban et al., “Low-voltage 60Gb/s NRZ and 100Gb/s PAM4 O-band silicon ring modulator,” in *Proc. IEEE Opt. Interconnects Conf.*, 2019, pp. 1–2, doi: [10.1109/OIC.2019.8714384](https://doi.org/10.1109/OIC.2019.8714384).
- [65] F. Hu et al., “Beyond 300Gbps silicon microring modulator with AI acceleration,” 2021, *arXiv:2111.05331*.

Jasmin Smajic (Senior Member, IEEE) received the M.Sc. and Ph.D. degrees in numerical computing and optimization of static and time-varying electromagnetic fields from the Faculty of Electrical Engineering and Computing, Zagreb, Croatia, in 1998 and 2001, respectively. After his postdoctoral research with ETH Zurich from 2002 to 2004 on the topic of full-Maxwell electromagnetic simulations of photonic crystals, he took a position of a Scientist with ABB Corporate Research Centre, Baden-Dättwil, Switzerland, where he stayed till 2011. His work with ABB covered a wide range of projects in the field of computational and applied electromagnetics. From 2011 to 2020, he was a Full Professor of electrical engineering with the University of Applied Sciences, Rapperswil, Switzerland, where he was leading Computational and Applied Electromagnetics Group. Since 2020, he has been a Senior Scientist with the Swiss Federal Institute of Technology, Zurich, Switzerland. He has authored more than 100 scientific publications, several books, and dozens of patents. He is a Member of CIGRE.

Juerg Leuthold received the Ph.D. degree in physics from ETH Zürich, Zürich, Switzerland, in 1998, for work in the field of integrated optics and all-optical communications. Since 2013, he has been the Head of the Institute of Electromagnetic Fields, ETH Zurich. From 2004 to 2013, he was with the Karlsruhe Institute of Technology, Karlsruhe, Germany, where he was the Head of the Institute of Photonics and Quantum Electronics and the Helmholtz Institute of Microtechnology. From 1999 to 2004, he was with Bell Labs, Lucent Technologies, Holmdel, NJ, USA, where he performed device and system research with III/V semiconductor and silicon optical bench materials for applications in high-speed telecommunications. His research interests include photonics, plasmonics, and microwave with an emphasis on applications in communications and sensing. Dr. Leuthold is a Fellow of the Optical Society of America and a member of the Heidelberg Academy of Science. He served the community as a member of the Helmholtz Association Think Tank, member of the Board of Directors of OSA, and in many technical program committees or as the General Chair of meetings.